Microelectronic Engineering 86 (2009) 2305–2311

Contents lists available at ScienceDirect

Microelectronic Engineering

journal homepage: www.elsevier.com/locate/mee

Electrical and interface properties of Au/DNA/*n*-Si organic-on-inorganic structures

Salih Okur [a,*], Fahrettin Yakuphanoglu [b], Mehmet Ozsoz [c], Pınar Kara Kadayifcilar [c]

[a] Department of Physics, Izmir Institute of Technology, Gulbahce Campus, Urla, Izmir 35430, Turkey
[b] Physics Department, Firat University, Elazig 23169, Turkey
[c] Department of Analytical Chemistry, Faculty of Pharmacy, Ege University, Bornova, Izmir 35100, Turkey

ARTICLE INFO

Article history:
Received 11 July 2008
Received in revised form 30 December 2008
Accepted 11 April 2009
Available online 22 April 2009

Keywords:
Organic/inorganic junction
DNA
Ideality factor

ABSTRACT

The effect of the thickness and coverage rate of a DNA film on the electrical and interface properties of Au/DNA/*n*-Si organic-on-inorganic structures has been investigated. The thin film properties of the DNA deposited on *n*-Si wafer were characterized by atomic force microscopy. The effect of the thickness and coverage rate of the DNA layer was investigated by evaluating electrical parameters, such as the barrier height, ideality factor, series resistance, and interface state density. The thickness and coverage rate of the DNA layer significantly affects the electrical properties of the Au/DNA/*n*-Si organic-on-inorganic structures. The interface state density properties of the Au/DNA/*n*-Si diodes were determined by conductance technique. The results show that the interface state density decreases with decrease in both film thickness and coverage rate of the DNA in an acetate buffer, modifying the electronic parameters of the Au/DNA/*n*-Si diodes.

© 2009 Elsevier B.V. All rights reserved.

1. Introduction

As a nano-device material for molecular biotechnology and nano-electronics, there are many advantages to using DNA such as the ability to control its size through base-pair manipulation and to achieve self-assembly [1–6]. Electrostatic interactions of DNA with positively charged surfaces are frequently considered in the literature [7,8]. A DNA molecule (a genetic information carrier) is a double-stranded negatively charged polymer. DNA adsorption at negatively charged surface using self-assembled molecular monolayer or Peptide Nucleic Acid treatments are also investigated [9]. DNA changes its conformation through environmental interactions with the other components of the living cells [10,11]. Several conduction mechanisms, such tunnelling (single-step super-exchange) [12], and hopping (multistep charge transport) [13], over guanine (G) as the DNA base with the lowest ionization potential were suggested for the electrical transport through DNA molecules. Thus, DNA has been shown to be an insulator, [14–16] a semiconductor, [13,17–19] a good conductor, [6] and a proximity-induced superconductor [20].

Controlling of electronic properties of metal/inorganic diodes is the key to fabricate reproducible metal/organic semiconductor/inorganic rectifying devices. Modifying the interface electronic states of the metal/inorganic semiconductor structure through DNA molecules can be essential for electronic devices for biotechnology related applications. This could lead to an efficient barrier height modification of the metal/semiconductor devices.

In several organic/inorganic Schottky diode studies [21–25], modification of the electronic parameters of the diodes by using various organic materials have been demonstrated. Nicollian and Brews suggested that the interface state density properties of the diodes can be determined using conductance technique [26]. In this work, we have modified the electronic interface states of the *n*-type Si Schottky diode with a DNA, and analyzed. The interface thin film properties of the DNA in the acetate buffer layer formed on *n*-Si were characterized by utilizing semi-contact tapping mode atomic force microscopy (TM-AFM).

AFM has been a widely used as a powerful research tool in molecular biology for analyzing the structures of bio-molecules such as proteins [27–29], DNA [30–32] and others [33,34]. AFM images sample surfaces by continuous scanning with a sharp tip. In simple contact mode AFM, a tip at the end of a flexible cantilever is used to detect sub-nanometer size changes in the interactional force as a function of height for the molecular surface, resulting in a 2-dimensional plot of topographic features [35,36]. In semi-contact tapping mode atomic force microscopy (TM-AFM), the topographic image is collected from any type of (hard or soft) surface with an oscillating probe tip driven near its resonance frequency by a piezoelectric transducer that provides a driving force of a constant amplitude [37,38]. During TM-AFM scanning, an oscillating tip comes so close to the sample surface that, it regularly touches the surface for a very short period of time during its oscillations. The short tip-sample contact time prevents any irreversible destruction on soft surfaces. The relatively weak tip-sample interaction becomes stronger as the tip approaches the surface and it lowers the vibrational amplitude by creating a phase shift between measured and actuating signal [39]. The AFM electronic feedback system maintains the amplitude of

* Corresponding author. Tel.: +90 232 750 7706; fax: +90 232 750 7707.
E-mail address: salihokur@iyte.edu.tr (S. Okur).

0167-9317/$ - see front matter © 2009 Elsevier B.V. All rights reserved.
doi:10.1016/j.mee.2009.04.017

tip oscillations at a user-defined set point (the operating amplitude) during construction of the surface topography. Obtaining an image of the phase signal simultaneously with the topographical mapping of the sample surface (known as the phase contrast method) provides additional information on the details of the surface structure. While the cantilever operating in the tapping mode gives topographical information via Van der Waals interactions, i.e., a combination of long-range attractive and short-range repulsive forces [40,41], the phase image allows mapping of the variation of surface properties such as composition, adhesion, friction, and visco-elasticity [42,43].

In the present study, the effect of the thickness and coverage rate of the DNA on the acetate (ABS) buffer layer on the electronic interface states of Au/DNA/*n*-Si organic-on-inorganic Schottky diodes was investigated by evaluating electrical parameters such as the barrier height (ϕ_b), ideality factor (n), series resistance (R_s), and interface state density (D_{it}) from conductance and capacitance measurements.

2. Experimental details

In this work, an *n*-type (N/Phos) single crystal silicon wafer pre-polished on one side and having a ⟨1 0 0⟩ surface orientation, thickness of 0.530 mm, diameter of 100 mm and 2.00 Ohm-cm resistivity was purchased from Si-Mat Silicon Wafers Company, and used as a substrate. The Si wafer was cleaned for 10 min in boiling trichloroethylene, acetone, and ethanol, consecutively. Then, it was cleaned using the following series of solvent or solvent mixtures: H_2SO_4, H_2O_2, HF: H_2O (1:20) solution, HNO_3:HF:H_2O (6:1:35), and finally a HF: H_2O (1:20) solution. The Si wafer was rinsed thoroughly in de-ionized water of 18 M before and after cleaning with each solvent or solvent mixture. The fish sperm DNA (as lyophilized powder) was obtained from Serva Company (Germany). The double-stranded DNA (dsDNA) stock solution (1000 mg/L) was prepared with ultra pure distilled water and kept frozen. More dilute solutions of dsDNA were prepared in 0.05 M acetate buffer solutions, each containing 20 mM NaCl (ABS, pH 4.80). The DNA sample was diluted to 10 and 0.1 mg/L with the ABS solution. Immediately after surface cleaning, 6 μl of the DNA solutions at three different concentrations were coated by the drop casting method and allowed to dry 12 h in a humid-free desiccator. The DNA organic film thickness and homogeneity depends on its solution concentration and wetting property on the *n*-type Si substrate. Using the AFM scratch and measure method, average DNA film thicknesses of 200 and 50 nm for DNA volumetric concentrations of 10 and 0.1 mg/L, respectively were determined for the samples.

In a turbo pumped high vacuum system at a pressure of 5×10^{-6} Torr, Au (99.9% purity) with a thickness of 200 nm was thermally evaporated from a tungsten filament using a mask of 2 cm diameter to form the top contact on the DNA film surface of the Si wafer. The back side of the Si substrate had been polished with high speed rotating sand paper to remove the native oxide and to create an ohmic contact before the 200 nm Au thin film deposition. The current–voltage (*I–V*) characteristics of the Au/DNA/*n*-Si diodes were performed with a Model 2400 KEITHLEY (Cleveland, USA) source-meter and a GPIB data transfer card for current–voltage measurements. The capacitance–voltage measurements were measured using a Model 3532 HIOKI HITESTER LCR meter (Bohemia, USA).

DNA samples were visualized with a Solver P47H atomic force microscope (NT-MTD, Moscow, Russia) operating in the tapping mode in air at room temperature. A scanner, equipped with a scanning piezoelectric element (piezo scanner) with maximum scan range of 4 μm × 4 μm × 1.5 μm was used to obtain both surface morphology and phase images of the DNA films that had been coated by the drop casting method on a *n*-type Si substrate. Special diamond-like carbon (DLC) coated NSG01_DLC silicon cantilevers (NT-MTD) with a 2 nm tip apex curvature, a length of 130 μm, a spring constant of 5.5 N/m, and a resonance frequency of 150 kHz was used to take the topographies during the AFM scanning. The scan resolution was 512 × 512 pixels. The images were processed by the linear flattening method in order to remove the background slope. The Nova 914 software package was used for controlling the SPM system and analyzing the AFM images.

3. Results and discussion

3.1. AFM results of the DNA thin films deposited on Si substrate

In this work, the AFM tapping mode phase imaging (TM-AFMPI) was used to distinguish the DNA molecular film layer from the ABS buffer. When imaging DNA molecules by AFM on any smooth surface, the DNA concentration has to be prepared so low that the individual DNAs can be found easily on the scanned surface separated from each other. In our case, two different concentrations have been prepared to investigate film formation properties of the DNA in ABS buffer on *n*-type Si wafer surface, rather than visualizing the individual DNA molecules. Nevertheless around the edge of the drop casted DNA film, the individual DNA molecules could be seen separately. We have experienced that the DNA can not be imaged unless it is dried following the adsorption process. It aggressively interacts with the tip and changes the tip resonance frequency by loading extra mass as a result of sticking to the tip. But a few DNA molecules suspended on the tip enhances the interaction between the surface and the tip. The resolution of both topography and especially the phase image increases dramatically after a few scans on the DNA covered film surface.

The AFM topography and AFM phase image of the 200 nm DNA film with the volume concentration of 10 mg/L on the ABS buffer surface are given in Fig. 1a and b, respectively. The color bars on the right sides show surface height and phase angle changes, respectively. The lighter regions have higher altitude on the 2D surface. On the other hand, the lighter regions on the phase image show that more repulsive interaction takes place between the tip and the DNA surface. The topography shows a smooth and completely covered DNA film surface, while the film disorders and pinholes of the DNA film can be distinguished from the contrast of the AFM phase image clearly. The DNA film thickness on ABS buffer layer was measured around 3 nm by taking a cross sectional height profile from one of the pinholes on the film surface as shown in Fig. 1c. The coverage rate of DNA film was obtained as 96% over the area of 3 μm × 3 μm of the film from the statistical calculations of the phase image as given in Fig. 1d.

Fig. 2a and b show the AFM topography and AFM phase image of the 50 nm DNA film with the volume concentration of 0.1 mg/L, respectively. The film disorders and coverage rate is more pronounced in both the topography and phase image. The lighter region represents the DNA film, while the darker region represents the underlying ABS buffer layer. The DNA film thickness on ABS buffer layer has been measured around 4 nm by taking a height profile across a line through edge of a pinhole on the DNA film surface as shown in Fig. 2c. In Fig. 2d, the statistical phase angle-frequency profile of the phase image shows 60% darker regions (buffer layer). The remaining 40% coverage can be deduced for the DNA film coverage over the area of 3 μm × 3 μm of the dried DNA film concentration of 10 and 0.1 mg/L.

3.2. The current–voltage characteristics of Au/DNA/n-Si diodes

Fig. 3 shows the current–voltage characteristics of the Au/DNA/*n*-Si diodes. The diodes show a rectifying behavior. The rectifying property of the Au/DNA/*n*-Si diode is improved with film thickness.

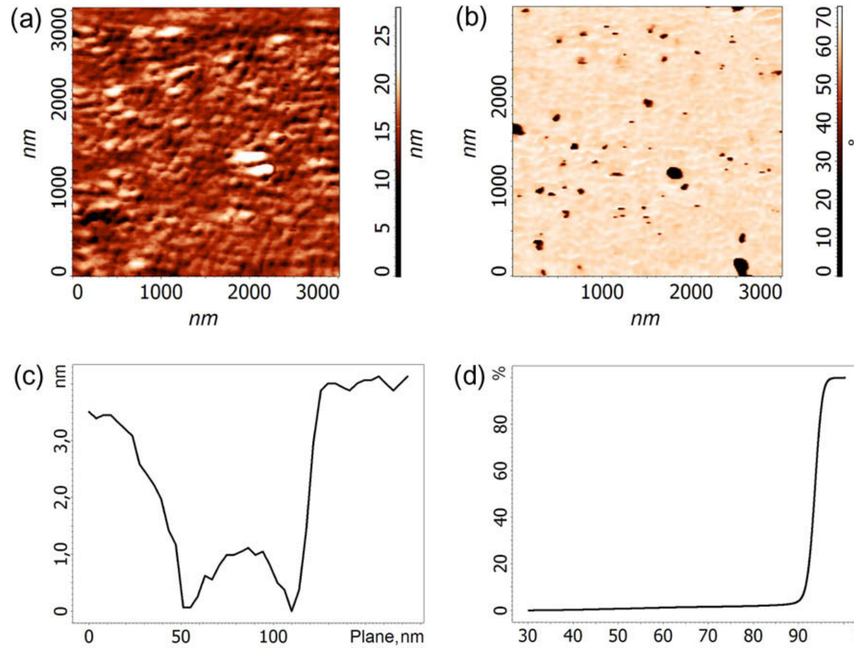

Fig. 1. (a) AFM topography of DNA, (b) AFM phase image of the 200 nm DNA film with the volume concentration of 10 mg/L in the ABS buffer layer on n-Si surface, (c) the cross-sectional profile of DNA taken from a pinhole on the film, and (d) the coverage rate of DNA is obtained as 96% over a scan area of 3 μm × 3 μm of the film.

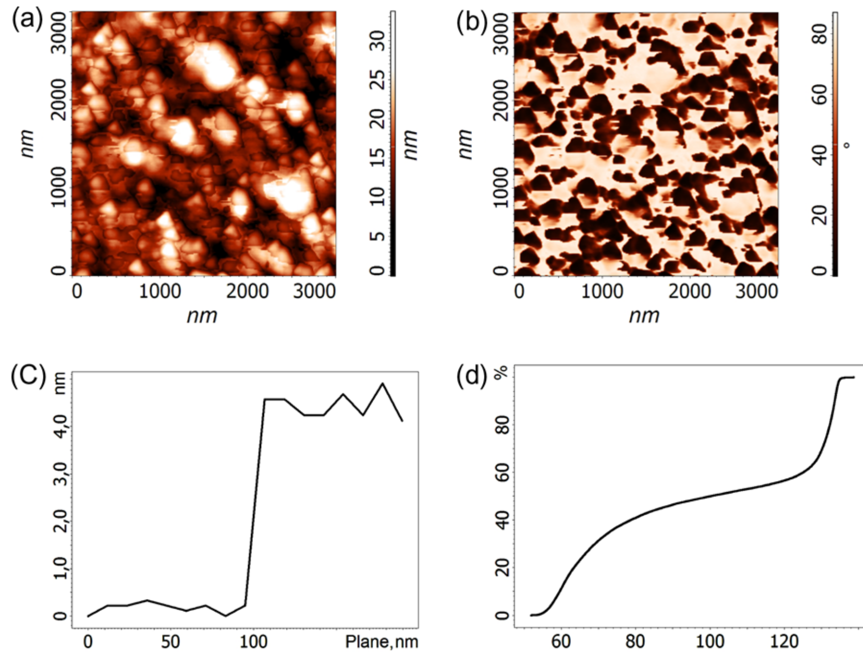

Fig. 2. (a) AFM topography of DNA, (b) AFM phase image of the 50 nm DNA film with the volume concentration of 0.1 mg/L in the ABS buffer layer on n-Si surface, (c) the cross-sectional DNA profile taken from edge of the film, and (d) the coverage rate of DNA is obtained as 40% over a scan area of 3 μm × 3 μm of the film.

The current–voltage characteristics of the diodes can be analyzed by the following relation [44],

$$I = I_o \exp\left(\frac{q(V - IR_s)}{nkT}\right)\left[1 - \exp\left(-\frac{q(V - IR_s)}{kT}\right)\right] \quad (1)$$

where n is the ideality factor, k is the Boltzmann constant, R_s is the series resistance, V is the applied voltage, T is the temperature and I_o is the reverse saturation current. The ideality factors of the diodes were determined from the I–V characteristics. The ideality factors are higher than unity due to the DNA film with ABS layer and possible thin oxide layer and series resistance at the interface. The oxide layer at the interface may be formed during surface preparation of the Au evaporation. The presence of interfacial layer, series resistance effect and bulk resistance of the DNA film affects the electronic parameters of the organic–inorganic structures. In order to analyze the series resistance effect, we have used Cheung's method to determine the diode parameters with the Cheung's functions expressed as [45],

$$\frac{dV}{d\ln(I)} = n\frac{kT}{q} + IR_s \quad (2)$$

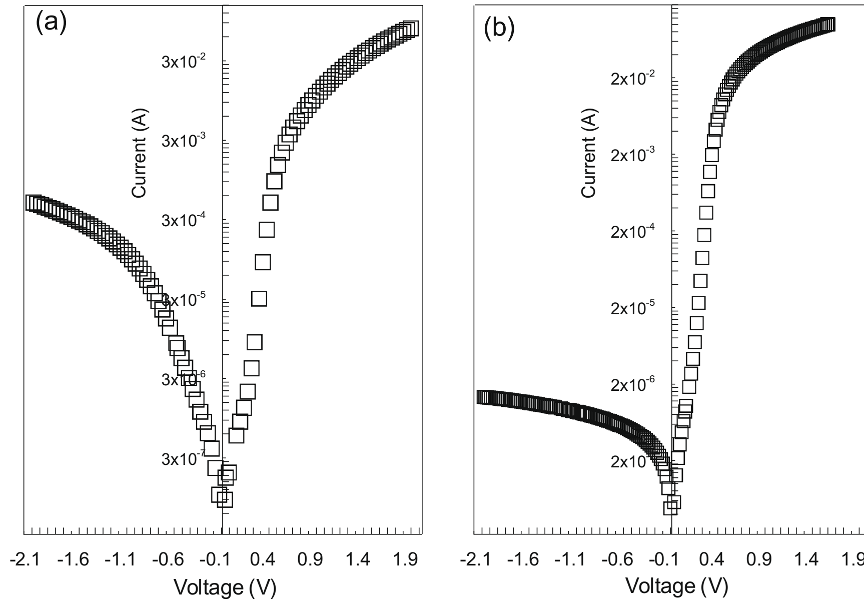

Fig. 3. Current–voltage characteristics of the Au/DNA/*n*-Si diodes (a) for 200 nm film layer, and (b) for 50 nm film layer.

and

$$H(I) = V - n\frac{kT}{q}\ln\left(\frac{I_o}{AA^*T^2}\right) = IR_s + n\phi_b \qquad (3)$$

where I_o is the saturation current, A is the contact area, A^* is the Richardson constant (112 A cm^{-2} K^{-2} for *n*-Si) [46], R_s is the series resistance and ϕ_b is the barrier height. The plots of $dV/dlnI$ vs. I and $H(I)$ vs. I of the diodes are shown in Fig. 4a and b and the obtained parameters are given in Table 1. The R_s and n values were calculated from the slope and intercept of the $dV/d\ln I$ vs. I plot and the results are given in Table 1. The series resistance is decreased with decreasing film thickness. This suggests that the low value of series resistance obtained for the diodes with thinner DNA layer gives a Schottky diode with better performance. The ideality factor n and barrier height ϕ_b values are higher for the thicker DNA layer (200 nm). This indicates that organic film thickness affects the ideality factor and barrier height. Furthermore, at intermediate and higher voltages, the organic layer may change the charge transport mechanism of the diode. Thus, to be sure about this, *I–V* characteristics of the diodes were plotted in logarithmic scale, as shown in Fig. 5. The logarithmic *I–V* curves in the figures indicate three different current regions exhibiting the power law behavior of $I \sim V^m$, where m shows the slope of each region. The m values for regions I, II and region III of the Au/DNA (200 nm)/*n*-Si and Au/DNA (50 nm)/*n*-Si were found to be 1.08, 8.91, 3.01 and 1.34, 10.48, 2.03, respectively. The obtained m values correspond to ohmic, trapped charge-limited current (TCLC), and space charge-limited current (SCLC) mechanisms. The third region for the diodes is transformed from TCLC to SCLC mechanism with decrease in DNA film thickness. In the TCLC mechanism, the current is controlled by exponential distribution of traps in the band gap of the DNA layer. The obtained results reveal that the film thickness and coverage rate of the DNA layer modifies the *I–V* characteristics of the diode as a result of various charge related conduction mechanisms in the Au/DNA/*n*-Si diode.

3.3. Interface state density properties of the Au/DNA/n-Si diodes

The plots of capacitance vs. frequency under bias voltages of 0 and 0.5 V are shown in Fig. 6. The capacitance decreases with increasing frequency and tends to non-dispersive. At lower frequencies, the capacitance increases with decreasing frequency. This is an indication of presence of a continuous distribution of the interface states. The non-dispersive behavior of capacitance suggests that the interface states in equilibrium with the semiconductor do not contribute to the capacitance. In the non-dispersive region, the charges at the interface states cannot follow the fast alternating current signal. The capacitance at lower frequencies corresponds to the sum of space-charge capacitance and interface capacitance, while at higher frequencies the total capacitance arises mostly from the space-charge capacitance [43].

For the conductance model, the parallel capacitance C_p and conductance G_p relations are expressed as [45],

$$C_p = C_s + \frac{C_{it}}{1 + (\omega\tau_{it})^2} \qquad (4)$$

and

$$\frac{G_p}{\omega} = \frac{q\omega\tau_{it}D_{it}}{1 + (\omega\tau_{it})^2} \qquad (5)$$

where $C_{it} = qD_{it}$, $\tau_{it} = R_{it}C_{it}$ and τ_{it} is the interface trap constant. The normalized conductance is expressed as,

$$\frac{G_p}{\omega} = \frac{qAD_{it}\tau_{it}}{2\omega\tau_{it}}\ln(1 + \omega^2\tau_{it}^2) \qquad (6)$$

where D_{it} is the density of the interface states, q is the charge of the electron, ω is the angular frequency, τ is the time constant of the interface states. The parallel conductance between measured conductance and capacitance is expressed as following,

$$\frac{G_p}{\omega} = \frac{\omega G_m C_{ox}^2}{G_m^2 + \omega^2(C_{ox} - C_m)^2} \qquad (7)$$

where C_{ox} is the capacitance of oxide layer, G_m and C_m are measured conductance and capacitance respectively. The interface state density is determined using the following relation,

$$D_{it} = \frac{(G/\omega)_{\max}}{0.402qA}. \qquad (8)$$

Fig. 7 shows the plots of (G/ω) vs. f of the diode at different bias voltages. The plots indicate a peak due to the presence of interface states. The shift in the peak position to higher frequencies with

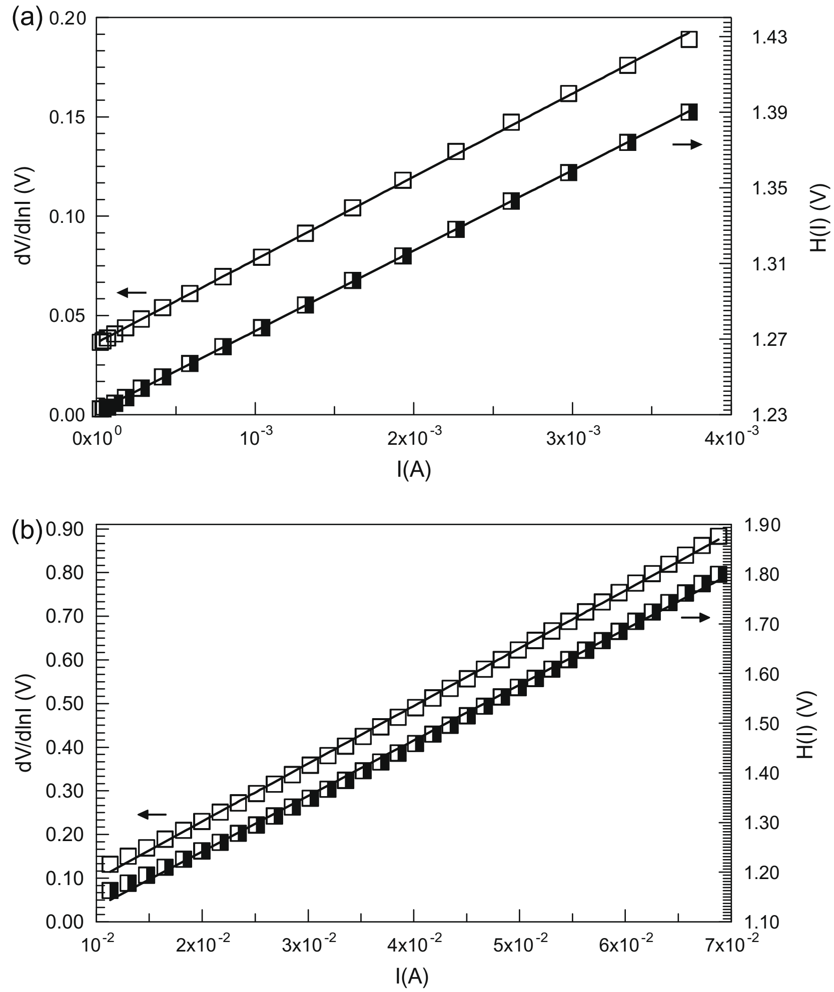

Fig. 4. Plots of $dV/d\ln(I)$ vs. I and $H(I)$ vs. I of the Au/DNA/n-Si diodes (a) for 200 nm film layer, and (b) for 50 nm film layer.

Table 1
Electronic parameters of the diodes.

Diode	n	$^{C-V}\phi_b$ (eV)	$^{I-V}\phi_b$ (eV)	$^{dV/d\ln I}R_s$ (Ω)	$^{H(I)}R_s$ (Ω)	D_{it} (eV cm^{-2})
Au/DNA(200 nm)/n-Si	1.41	1.35	0.87	41.84	42.51	8.56×10^{12}
Au/DNA(50 nm)/n-Si	1.35	1.17	0.75	13.23	11.19	2.54×10^{12}

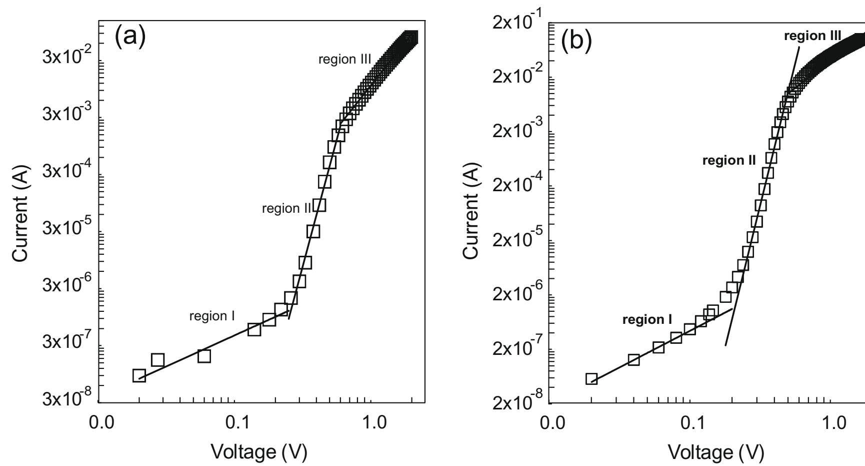

Fig. 5. Current–voltage characteristics in logarithmic scale of the Au/DNA/n-Si diodes (a) for 200 nm film layer, and (b) for 50 nm film layer.

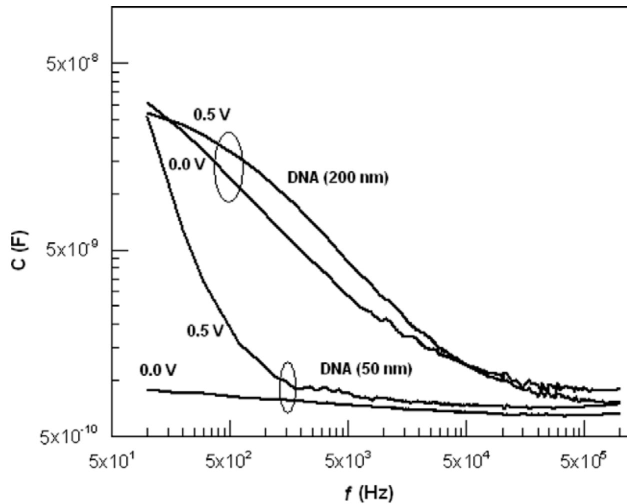

Fig. 6. Plots of C–f of the Au/DNA/n-Si diodes.

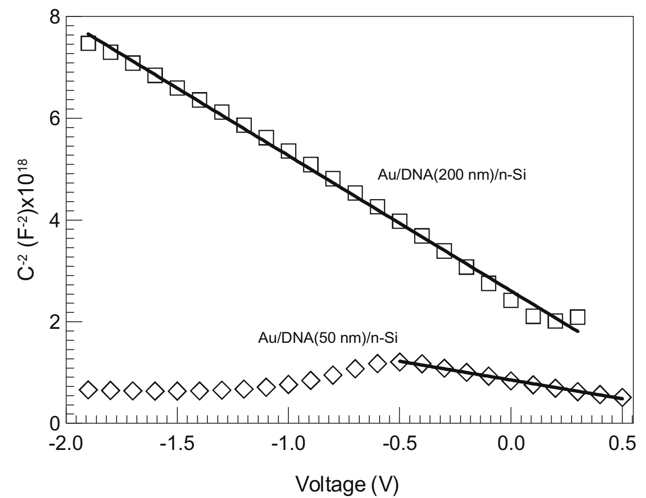

Fig. 8. Plot of C^{-2}–V of the Au/DNA/n-Si diodes.

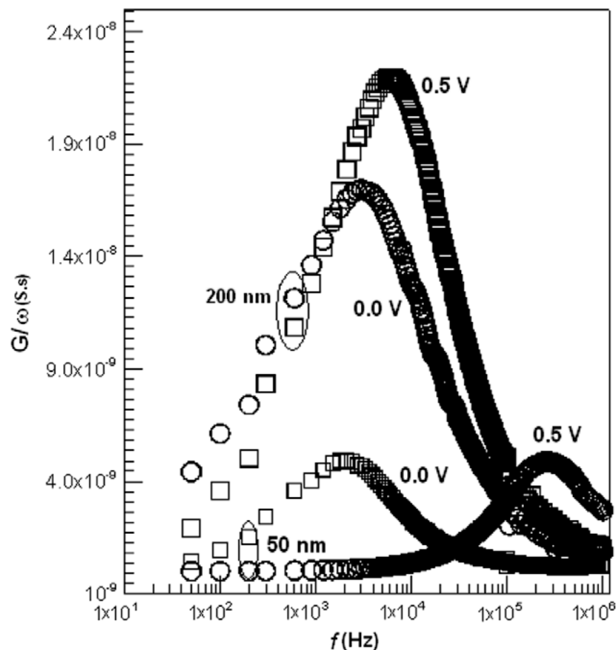

Fig. 7. Plots of G/ω–f of the Au/DNA/n-Si diodes at bias various voltages.

increasing bias voltage suggests that the time constant of interface states is decreased with applied voltage. The calculated density of interface state (D_{it}) of the Au/DNA/n-Si diodes is given in Table 1. The decrease in the D_{it} value of the Au/DNA/n-Si diode with decreasing film thickness suggests that the electronic parameters are improved with decreasing interface state density as a result of lower coverage rate of DNA molecules in the interface.

3.4. Capacitance–voltage characteristics of the Au/DNA/n-Si diodes

Fig. 8 shows the capacitance–voltage (C–V) curves of the Au/DNA/n-Si diodes at 100 kHz. The C–V curves of the diodes were plotted in the form of C^{-2}–V and are given in Fig. 8. The C^{-2} vs. V plot of the Au/DNA (50 nm)/n-Si diode gives a shorter flat region, whereas for the diode having thicker DNA thickness gives a longer flat region. This shows that the uniformity of the interface of the diode is improved with the thicker film thickness. The capacitance–voltage characteristics of the diode can be analyzed by the following relation [47],

$$\frac{1}{C^2} = \frac{2(V_{bi} + V)}{A^2 \varepsilon_s q N_d} \tag{9}$$

where V_{bi} is the built-in potential, ε_s is the dielectric constant of semiconductor (11.7 for Si) [47] and N_d is the donor concentration. The barrier height ϕ_b can be obtained by the following relation,

$$q\phi_{B(C-V)} = qV_{bi} + kT \ln\left(\frac{N_c}{N_d}\right) \tag{10}$$

where N_c is the effective density of state in the conduction band of silicon ($N_v = 2.8 \times 10^{19}$ cm^{-3}).

N_d and V_{bi} values for the diodes were calculated from the slope and intercept of C^{-2}–V plot. The barrier height ϕ_b values of the diodes were calculated using the obtained N_d and V_{bi} values. The ϕ_b value of the diode for the thin DNA layer (50 nm) is low in comparison to that of the thicker DNA layer (200 nm). This indicates that the film thickness reduces the barrier height of the n-Si/DNA/Au diodes. The $\phi_{b(C-V)}$ value is obtained higher than the $\phi_{b(I-V)}$ value due to the barrier inhomogeneities of the interfacial layer thickness and distributions of the interfacial charges [48,49]. Furthermore, this also shows the I–V and C–V characteristics have different nature. Thus, the barrier heights obtained from I–V to C–V measurements are not the same [50].

4. Conclusions

The interface structure and electrical properties of Au/DNA/n-Si organic-on-inorganic structure have been investigated by atomic force microscopy, current–voltage and capacitance–voltage methods. The thickness and coverage rate of the DNA layer significantly affect electrical parameters such as the, barrier height (ϕ_b), ideality factor (n), series resistance (R_s) and interface state density (D_{it}) of the Au/DNA/n-Si organic-on-inorganic structures. The interface state density for the Au/DNA/n-Si diodes was found to be $\sim 10^{12}$ (eV cm^{-2}) and interface state density decreases with the decrease in film thickness. The low value of series resistance and interface state density gives the high performance of the Au/DNA/n-Si organic-on-inorganic diode for thin DNA layer thickness.

Acknowledgements

This study was financially supported by Turkish State Planning Organization (DPT) with the research project number DPT2003K120390. Dr. Ritchie Eanes is acknowledged for his technical and grammatical proof reading suggestions.

References

[1] C.A. Mirkin, R.L. Letsinger, R.C. Mucic, J.J. Storhoff, Nature (London) 382 (1996) 607.
[2] S.J. Tans, A.R.M. Vershueren, C. Dekker, Nature (London) 393 (1998) 49.
[3] C.J. Murphy, M.R. Arkin, Y. Jenkins, N.D. Ghatlia, S.H. Bossmann, N.J. Turro, J.K. Barton, Science 262 (1993) 1025.
[4] Y. Okahata, T. Kobayashi, K. Tanaka, M. Shimomura, J. Am. Chem. Soc. 120 (1998) 6165.
[5] Y. Maeda, H. Tabata, T. Kawai, Appl. Phys. Lett. 79 (2001) 1181.
[6] M.A. Reed, C. Zhou, C.J. Muller, T.P. Burgin, J.M. Tour, Science 278 (1997) 141.
[7] C.R. Clemmer, T.P. Beebe, Scann. Microsc. 6 (1992) 319.
[8] H.G. Hansma, I. Revenko, K. Kim, D.E. Laney, Nucl. Acids Res. 24 (1996) 713.
[9] M. Fojta, V. Vetterl, M. Tomschik, F. Jelen, P. Nielsen, J. Wang, E. Palecek, Biophys. J. 72 (1997) 2285.
[10] S. Takeishi, J. Chem. Phys. 120 (2004) 550.
[11] S.M. Parsons, J. Struct. Biol. 119 (1997) 99.
[12] B. Giese, J. Amaudrut, A.K. Kohler, M. Spormann, S. Wessely, Nature 412 (2001) 318.
[13] D. Porath, A. Bezryadin, S. de Vries, C. Dekker, Nature 403 (2000) 635.
[14] E. Braun, Y. Eichen, U. Sivan, G. Ben-Yoseph, Nature 391 (1998) 775.
[15] P.J. de Pablo, F. Moreno-Herrero, J. Colchero, J.G. Herrero, P. Herrero, A.M. Baro, P. Ordejon, J.M. Soler, E. Artacho, Phys. Rev. Lett. 85 (2000) 4992.
[16] Y. Zhang, R.H. Austin, J. Kraeft, E.C. Cox, NP. Ong, Phys. Rev. Lett. 89 (2002) 198102.
[17] K.H. Yoo, D.H. Ha, J.O. Lee, J.W. Park, J. Kim, JJ. Kim, H.Y. Lee, T. Kawai, H.Y. Choi, Phys. Rev. Lett. 87 (2001) 198102.
[18] J.S. Hwang, K.J. Kong, A. Ahn, G.S. Lee, D.J. Ahn, S.W. Hwang, Appl. Phys. Lett. 81 (2002) 1134.
[19] B. Hartzell, B. McCord, D. Asare, H. Chen, J.J. Heremans, V. Soghomonian, Appl. Phys. Lett. 82 (2000) 4800.
[20] J.R. Heath, P.J. Kuekes, G.S. Snider, R.S. Williams, Science 280 (1998) 1716.
[21] I.H. Campbell, S. Rubin, T.A. Zawodzinski, J.D. Kress, R.L. Martin, D.L. Smith, Phys. Rev. B 54 (1996) 14321.
[22] T. Kılıçoğlu, Thin Solid Films 516 (2008) 967.
[23] F. Yakuphanoglu, Sensors Actuat. A 141 (2008) 383.
[24] Ş. Aydoğan, M. Sağlam, A. Türüt, Microelectr. Eng. 85 (2008) 278.
[25] M.E. Aydin, F. Yakuphanoglu, T. Kılıçoğlu, Synth. Met. 157 (2007) 1080.
[26] E.H. Nicollian, J.R. Brews, MOS (Metal Oxide Semiconductor) Physics and Technology, Wiley, New York, 1982.
[27] A. Brisson, W. Bergsma-Schutter, F. Oling, O. Lambert, I. Reviakine, J. Cryst. Growth 196 (1999) 456.
[28] I. Reviakine, A. Simon, A. Brisson, Langmuir 16 (2000) 1473–1477.
[29] M.E. Gracheva, A.L. Xiong, A. Aksimentiev, K. Schulten, G. Timp, J.P. Leburton, Nanotechnology 17 (2006) 622.
[30] J.B. Heng, C. Ho, T. Kim, R. Timp, A. Aksimentiev, Y.V. Grinkova, S. Sligar, K. Schulten, G. Timp, Biophys. J. 87 (2004) 2905.
[31] J. Lagerqvist, M. Zwolak, M. Di Ventra, Nano Lett. 6 (2006) 779.
[32] J. Vesenka, M. Guthold, C.L. Tang, D. Keller, E. Delaine, C. Bustamante, Ultramicroscopy 42–44 (1992) 1243–1249.
[33] I.A. Mastrangelo, M. Bezanilla, P.K. Hansma, P.V.C. Hough, H.G. Hansma, Biophys. J. 68 (1994) 293.
[34] Y. Fang, J. Yang, J. Phys. Chem. Ser. B 101 (1997) 441.
[35] G. Binnig, C. Gerber, E. Stoll, R.T. Albrecht, C.F. Quate, Europhys. Lett. 3 (1987) 1281.
[36] G. Schitter, R. Stark, W. Stemmer, Ultramicroscopy 100A (2004) 253.
[37] H.G. Hansma, J. Hoh, Annu. ReV. Biophys. Biomol. Struct. 23 (1994) 115.
[38] M. Luna, J. Colchero, A.M. Baro, Appl. Phys. Lett. 72 (1998) 3461.
[39] F. Moreno-Herrero, P.J. De Pablo, J. Colchero, J. Gomez-Herrero, A.M. Baro, Surf. Sci. 453 (2000) 152.
[40] J. Kokavecz, O. Marti, P. Heszler, A. Mechler, Phys. Rev. B 73 (2006) 15.
[41] G.R. Jayanth, Y. Jeong, C.H. Menq, Rev. Sci. Instrum. 77 (2006) 5.
[42] S.N. Magonov, V. Elings, V.S. Papkov, Polymer 38 (1996) 297.
[43] H.G. Hansma, K.J. Kim, D.E. Laney, R.A. Garcia, M. Argaman, S.M. Parsons, J. Struct. Biol. 119 (1997) 99.
[44] S.K. Cheung, N.W. Cheung, Appl. Phys. Lett. 49 (1986) 85.
[45] Ş. Karataş, A. Türüt, Vacuum 74 (2004) 45–53.
[46] E.H. Rhoderick, R.H. Williams, Metal-Semiconductor Contacts, second ed., 1988, p. 411.
[47] S.M. Sze, Physics of Semiconductor Devices, second ed., John Wiley & Sons Inc., Wiley, NewYork, 1981. p. 431.
[48] E.H. Nicollian, A. Goetzberger, Appl. Phys. Lett. 7 (1965) 216.
[49] Y.P. Song, R.L. Van Meirhaeghe, W.H. Laflere, F. Cardon, Solid State Electron. 29 (6) (1986) 633.
[50] Ö. Güllü, Ö. Barış, M. Biber, A. Türüt, Appl. Surf. Sci. 254 (2008) 3039.